Research Square

Preprints are preliminary reports that have not undergone peer review.
They should not be considered conclusive, used to inform clinical practice,
or referenced by the media as validated information.

Unsteady Surface Pressure Measurements on a Laminar Wing submerged in a Propeller Slipstream

Julian Geiger

julian.geiger@iag.uni-stuttgart.de

Universität Stuttgart

N. Konrad

Universität Stuttgart

U. Deck

Universität Stuttgart

Research Article

Keywords: Propeller-Wing Interaction, Surface Pressure Measurements, Experimental Fluid Mechanics, Distributed Propulsion

Posted Date: October 30th, 2026

DOI: https://doi.org/10.21203/rs.3.rs-11388382/v1

License: This work is licensed under a Creative Commons Attribution 4.0 International License.
Read Full License

Additional Declarations: No competing interests reported.

Unsteady Surface Pressure Measurements on a Laminar Wing submerged in a Propeller Slipstream

J. Geiger*, N. Konrad*, U. Deck*

High-frequency surface pressure measurements on a Natural Laminar Flow (NLF) airfoil submerged in the wake of a propeller were conducted in the Laminar Wind Tunnel (LWT) of the Institute of Aerodynamics and Gas Dynamics (IAG) of the University of Stuttgart. Based on the measured unsteady pressure signals, the laminar-to-turbulent transition on the airfoil is investigated. The resulting data can be used to further understand the interactions between a tractor-propeller and the boundary-layer (BL) flow. By gaining insights into BL-flow behaviour under such conditions, more efficient airplane propulsion and wing designs could become viable.
With the aid of high-frequency pressure sensors, it is possible to create a 2-dimensional resolution of the boundary layer state, along the spanwise position behind the traversable propeller and the chord of the airfoil. At certain advance ratios, laminar regimes are recorded reaching up to $x/c = 80\,\%$, far beyond the steady chord transition location of the NLF configuration. Depending on the advance ratio, the mean portion of laminar flow still varies in between $35 - 44\,\%$, corresponding to $63 - 81\,\%$ of the NLF distance of the steady reference configurations without a propeller installed. This clearly demonstrates the importance of considering the partly laminar boundary-layer flow behaviour on the airfoil, even when submerged in a propeller wake.
Keywords Propeller-Wing Interaction; Surface Pressure Measurements; Experimental Fluid Mechanics; Distributed Propulsion

List of Symbols

α	Angle of attack	$^\circ$
γ	Intermittency	$-$
ϕ	Propeller angle	$^\circ$
c	Chord length	m
f	frequency	Hz
J	Advance ratio	$-$
n	Number of revolutions	rps
R	Radius	m
Re	Reynolds number	$-$
p	Pressure	Pa
P_{pp}	Power Spectral Density of the pressure signal	Pa^2/Hz
S	Scatter value	Pa
u, v, w	Velocity components in Cartesian coordinates	m/s
x, y, z	Cartesian coordinates	m
$\langle\rangle$	Phase average	$-$
$\bar{}$	Temporal mean	$-$
$'$	Stochastic residual	$-$

Abbreviations

ADC	Analog-to-Digital Converter
BL	Boundary Layer
DP	Distributed Propulsion
IAG	Institute of Aerodynamics and Gas Dynamics
LWT	Laminar Wind Tunnel
NLF	Natural Laminar Flow
PSD	Power Spectral Density
TS	Tollmien-Schlichting

Acknowledgments and Declarations

The authors gratefully acknowledge the support of the Deutsche Forschungsgemeinschaft (DFG) under the project ID 498601949 - TRR 364.

The authors have no competing interests to declare that are relevant to the content of this article.

Julian Geiger
julian.geiger@iag.uni-stuttgart.de
https://orcid.org/0009-0000-0640-2519

* Universität Stuttgart, Institut für Aerodynamik und Gasdynamik, Pfaffenwaldring 21, 70569 Stuttgart, Deutschland

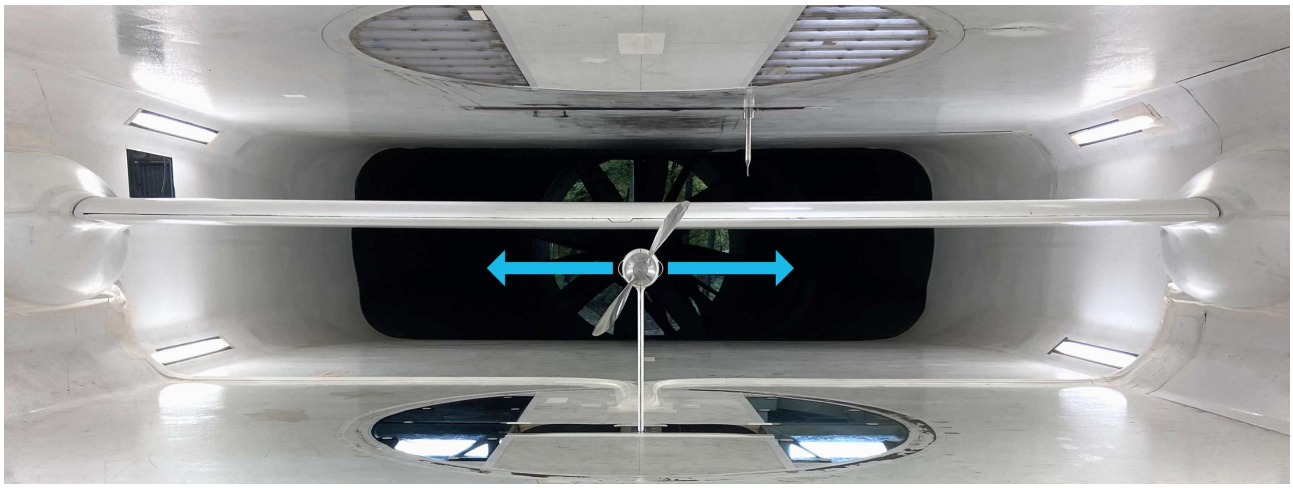


Fig. 1: Experimental setup in the LWT

1 Introduction

As environmental awareness grows in all areas of society, it is also growing in the aviation sector. More efficient, as well as electric propulsion systems are being investigated for future generations of aircraft. The research collaboration *SynTrac*[1] *TRR 364* is attempting to lay the foundation for just that. In an effort to integrate all aspects of an aircraft into the earliest development stages, researchers from a variety of fields are investigating these aspects to further their understanding. In this context, an aircraft with Distributed Propulsion (*DP*) in a tractor configuration is a very promising concept and is therefore considered. The subproject "B02-Utilizing the aerodynamic interaction between the propeller and the aircraft through an integrated design" was founded to analyze the boundary-layer (*BL*) behaviour of the propeller-altered flow around the airfoil. For this wind tunnel test in particular, the interactions of a single tractor propeller with a laminar wing are studied. The characterization of the boundary-layer state, measured via surface pressure variations, in such a configuration is presented in this paper. The same measurement procedure was repeated for three different propellers with differing advance ratios to investigate the effects of these variations on the boundary-layer response.

In a review of DP concepts, *Kim et al.* [12] summarized the benefits of this approach in lift generation, propulsive efficiency, acoustic effects, and new possibilities in vehicle control. *Deree et al.* [3] focused on simulations of a tractor-propeller DP design, varying the power conditions and rotational sense of the propellers. They found that corotating propellers, spinning counter to the tip vortex, have greater advantages for lift augmentation. Various demonstrators, such as *NASA's SCEPTOR* [1] and the e-Genius-mod VELAN [14] were developed to demonstrate the previously mentioned advantages of DP configurations.

Since propellers have been utilized in aviation for more than a century to this point, the first investigations into their interactions with wings began quite early as well. As early as 1921, the first experimental investigations on the mutual influence of propeller and wing were conducted by *Prandtl* [16], testing different configurations. While these studies focused on global effects, studies on the effect of the propeller slipstream on laminar-to-turbulent transition were already being conducted in the late 1930s and early 1940s, for example by *Hood & Gaydos* [9], *Wenzinger* [19] and *Zalovcik & Skoog* [20]. Using the quasi-static measurement techniques of their time, they concluded that the slipstream causes the transition point to move upstream towards the leading edge.

As unsteady measurement techniques became more available, the understanding of the underlying physics of the interaction started to become clearer. In an early work, *Miley et al.* [15] carried out detailed hot-wire measurements, highlighting the cyclic nature of the boundary-layer state relative to the propeller rotation rate. They also found that laminar flow design principles still applied and could be beneficial to performance. Later, free-flight measurements by *Horstmann et al.* [10], using hot-films, confirmed these findings. The cyclic behaviour was observed, and they found a drag reduction of 14 % in the slipstream compared to the fully turbulent value. Further investigations, such as those conducted by *Elsaadawy and Britcher* [4], came to the same con-

[1] Synergies of Highly Integrated Transport Aircraft

clusion of a periodic boundary layer state. *Catalano* [2] utilized both a wind tunnel model with an integrated pylon-propeller setup in a tractor configuration, as well as a disconnected pusher propeller. He found that the turbulence intensity within the boundary layer depended strongly on the employed blade count, and therefore on the passing frequency of the individual blades. However, high-frequency transition measurements were not performed, leading to an early transition being measured on average. *Halstead et al.* [8], experimenting on axial compressors and turbines, found the effectiveness of a *calmed region* in suppressing flow separation and delaying transition, in their case in the non-wake path. The *calmed region* being an area behind a passing wake or turbulent spot where Tollmien-Schlichting instabilities and bypass transition are suppressed, while transition occurs through interaction with other turbulent spots or strong bypass events [8]. According to *Schubauer and Klebanoff* [17] and *Halstead et al.* [8], this phenomenon occurs because the propagation velocity of Tollmien-Schlichting waves is slower than that of the trailing boundary of the turbulent event. Building upon previous findings, *Gostelow* studied the flow-physical effects in the area of turbulent spots in various publications and with various co-authors. First investigating the calmed region behind a turbulent spot [7], afterwards expanding the investigations to interactions of wake sheets with the boundary layer on a flat plate in an adverse pressure gradient and with a laminar separation bubble [6]. These investigations found that the calmed region was stronger behind a wake sheet than behind a turbulent spot. Additionally, the laminar separation bubble was suppressed during the passage of the wakes as well as for a finite period within the calmed region before reappearing [6].

2 Methods

A wind tunnel setup as described in [18] is used to investigate the unsteady transition location on a laminar wing in the *Laminar Wind Tunnel (LWT)* of the University of Stuttgart. The airfoil (*DP-FR-1924-MODLWT*, or *DLRmod12* for short) is mounted horizontally in the wind tunnel test section with an angle of attack of $\alpha = 2°$. Its chord length is $c = 0.35\,m$ and the corresponding target Reynolds number is $Re = 1.25 \cdot 10^6$. The propeller is mounted separately on a traversable pylon upstream of the airfoil without inclination relative to the oncoming flow, as shown in Figure 1.

The exact positions of the airfoil relative to the propeller and its pylon are given in Figure 2.

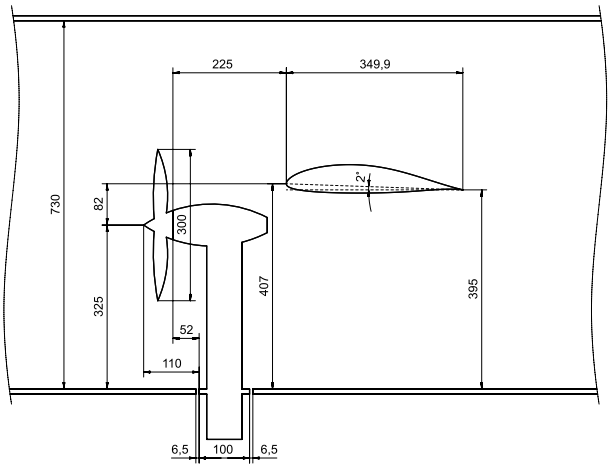


Fig. 2: Positioning of the airfoil and the propeller

30 *Kulite XCS-SL-062-±5D* pressure transducers with a pressure range of $\pm 350\,mbar$, an accuracy of $\pm 0.5\%$ of the full-scale range, and a natural frequency of $150\,kHz$ are connected to an array of pressure taps on the suction side of the airfoil via infinite-line (or infinite-tube) connections, as described by *Englund and Richards* [5]. They measure the differential pressure between the static pressure at the airfoil surface and the total pressure of the onflow upstream of the propeller.

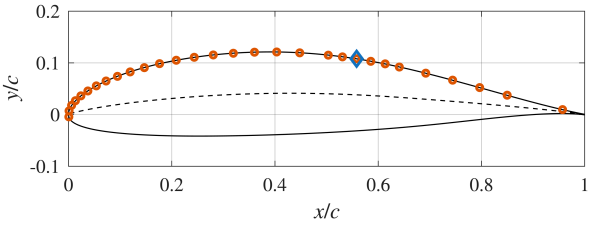


Fig. 3: Positions of the pressure taps on the airfoil

Figure 3 depicts the chordwise placement of the surface pressure taps as red circles.

Additionally, one Kulite is embedded directly into the airfoil surface at the same chordwise position as one of the pressure taps ($x/c = 55.8\,\%$), shown as a blue rhombus. It was implemented to provide a reference for the frequency response of the infinite-tube setup. This reference is then used as proof of the usability of the infinite-tube concept for unsteady pressure measurements. In the undisturbed, steady reference case, these two sensors are located just upstream of a laminar separation bubble.

Figure 4 provides a direct comparison of the power spectral densities (PSD) of the flush-mounted sensor and the sensor connected via an infinite tube

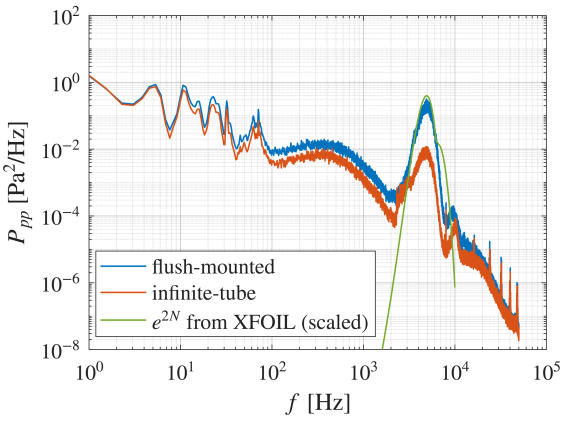


Fig. 4: Welch PSD, 1 s blocks, 50 % overlap, Hann window

at $x/c = 55.8\,\%$ in the undisturbed, steady case. The damping effect of the infinite-tube connection is clearly visible. At frequencies of several kHz, the damping seems to be strongest, reducing the signal by more than one decade. The peak around $5\,kHz$ can be associated with Tollmien–Schlichting (TS) waves, as confirmed by comparison with XFOIL data. As the peak is clearly visible even in the signal from the sensor connected via an infinite tube, it can be postulated that relevant phenomena, such as the TS waves observed here, are represented sufficiently well to be detected.

A *Precision Filters PF28000* signal conditioning unit is used both to amplify the signals received from the pressure transducers and to act as the bridge controlling the supply voltage of the sensors. To ensure a high temporal resolution, in addition to the infinite-tube setup, the data are recorded with a sample rate of 100 kHz by three synchronized *DT9857E-16-XAO* analog-to-digital converters (*ADCs*) from *Digilent co NI.*

The upstream located propeller can be traversed in the spanwise direction, allowing positions between $y/R = [-1, 1]$ to be investigated. To obtain a sufficiently fine spatial grid, a radius increment of $\Delta y/R = 0.1$ is chosen, resulting in 21 spanwise positions.

A *Megatron HTA36X* Hall sensor with an angular accuracy of $\pm 0.5°$ is used to calculate the rotational rate n and to determine the angular position of the propeller at every sample. However, the sensor updates its output at $5kHz$, a lower frequency than the recording rate, necessitating smoothing during post-processing to obtain a voltage signal suitable for further processing. The Hall sensor data enable phase averaging, allowing a matrix of $30(31) \times 21$ simultaneously measuring sensors to be emulated, although measurements at the individual radial positions and for each sensor are taken sequentially.

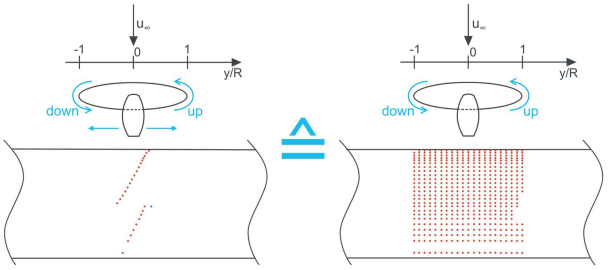


Fig. 5: Principle sketch of the method for creating a virtual sensor matrix

Figure 5 shows the principle used to emulate the matrix and the spanwise positioning of the pressure taps. The taps are not placed directly behind one another, preventing interactions that could distort the measurement data. The coordinate definition used is also visible in Figure 5: Positions behind the rising propeller blade are defined with $y/R > 0$, while positions behind the descending blade correspond to negative y/R values. Due to the differences in spanwise tap positions and the limited traversing length of the propeller, some sensors cannot measure at the outermost radial positions, as also shown in Figure 5.



Fig. 6: The three different propellers

Three different propellers are used during the measurements. The propellers differ in their advance ratio

$$J = \frac{u}{n \cdot D} \tag{1}$$

As all three propellers have the same Diameter of $D = 0.3\,m$, this means that they rotate at different rotational speeds n. This leads to different blade-passing frequencies. The propellers were designed to produce equal thrust at their respective design points, listed in Table 1. Although thrust was not

measured in the present wind tunnel campaign, this assumption is partly supported by measurements of the same propellers in a different wind tunnel, which showed reasonable agreement in the same order of magnitude among the three propellers [13]. However, similar thrust under the present test conditions cannot be confirmed directly.

propeller	RPM [1/min]	J [-]
Propeller 1	5000	2.14
Propeller 2	7500	1.43
Propeller 3	10000	1.06

Tab. 1: Design points of the different propellers

2.1 Assessment of the Boundary Layer State

In order to determine whether the boundary layer is laminar or turbulent based on the pressure signal, the moving scatter value

$$S = \sqrt{\frac{1}{N-1}\sum_{i=1}^{N}|x_i - \overline{x}|^2} \tag{2}$$

is applied as an approximation of the standard deviation. Here, N is the window size of the moving window, and $\overline{x}$ denotes the mean signal value within the current window. However, the steep periodic pressure jumps caused by the propeller also produce spikes in the scatter values. Due to the steepness of the pressure jumps, the desired effect of isolating turbulent fluctuations could not be achieved reliably with a high-pass filter. Therefore, a different approach is chosen. The phase-averaged pressure at the propeller position corresponding to each sample j is subtracted from the pressure value of that sample, $p(x,t)_j$. This approach is similar to the triple decomposition used by *Hussain and Reynolds* [11]:

$$p(x,t) = \overline{p}(x) + \tilde{p}(x,\phi) + p'(x,t) \tag{3}$$

Here, $\overline{p}$ is the time average of the entire signal, $\tilde{p}$ describes the deterministic (periodic) fluctuation, and p' is the remaining stochastic pressure fluctuation. The first two terms can be summarized as the phase average:

$$\langle p\rangle(x,\phi) = \overline{p}(x) + \tilde{p}(x,\phi) \tag{4}$$

Applying this principle to the discrete measurement data yields a *residual pressure signal* $p'(x,t)$, as given in Equation (5):

$$p'(x,t)_j = p(x,t)_j - \langle p\rangle(x,\phi_j) \tag{5}$$

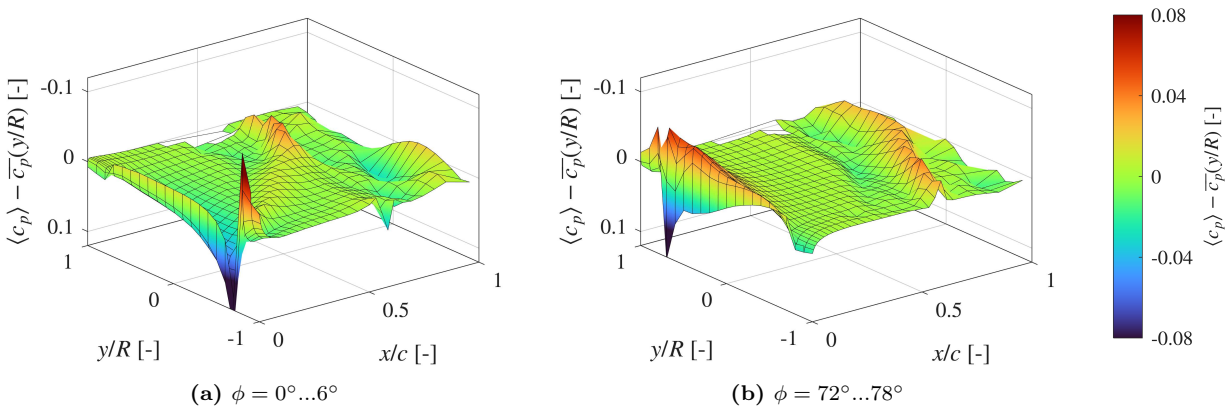
Subsequently, the moving scatter value of this residual pressure signal is calculated using a symmetrical window of 11 samples. The rotational positions of the propeller are then divided into bins of 6°. The scatter values within each bin are then averaged again to obtain the phase averaged scatter value $\langle S\rangle$. Based on an evaluation of reference configurations with a clean wing and a tripped boundary layer, a threshold of $S > 1,25\,Pa$ is set and evaluated for each sample. Values above the threshold are assumed to indicate turbulent or transitional flow, whereas values below the threshold indicate a laminar boundary-layer state.

3 Results

First, the unsteady pressure distributions exhibit the expected cyclic behaviour caused by the periodic passage of the propeller blades. The propagation of a propeller-induced pressure disturbance across the wing can be visualized by calculating the difference between the pressure coefficient at a given phase angle and its temporal mean. In Figure 7, this difference is plotted in two dimensions over x/c and y/R downstream of Propeller 1 for selected phase angles. On the suction side, except for the regions near the stagnation point, the static pressure drops as the propeller blade wake passes, followed by a slight pressure increase above the mean value. It then returns approximately to its mean. The magnitude of the pressure fluctuation is especially large in the regions close to the leading edge and downstream of a chord position of $x/c \approx 50\,\%$. At the stagnation point, the sign of the pressure change is reversed compared to that on the suction side. This appears to result from the higher dynamic pressure induced by the propeller blade, which leads to a higher static pressure at the stagnation point. Meanwhile, the excess velocity induced by the propeller leads to a lower static pressure on the suction side.

One main aspect of this study is the unsteady identification of laminar and turbulent or transitional regions of the boundary layer. The time history of the raw pressure signals from different pressure sensors alone already presents a very good impression of the boundary-layer behaviour. Once again, the cyclic nature of the flow becomes clear when looked at Figure 8.

Directly after the beginning of the blade wake passage, recognizable by the pressure jump, the signal fluctuations appear to be significantly larger. This effect is only visible at chordwise positions beyond approximately $x/c \approx 25\,\%$ of the total chord. Advancing toward the trailing edge, the fluctuations grow in both amplitude and duration. Shortly before the trailing edge, they begin to occupy the en-



(a) $\phi = 0°...6°$ **(b)** $\phi = 72°...78°$

Fig. 7: Deviation of the phase-averaged pressure coefficient $\langle c_p \rangle$ from its temporal mean value $\overline{c_p}$, Propeller 1

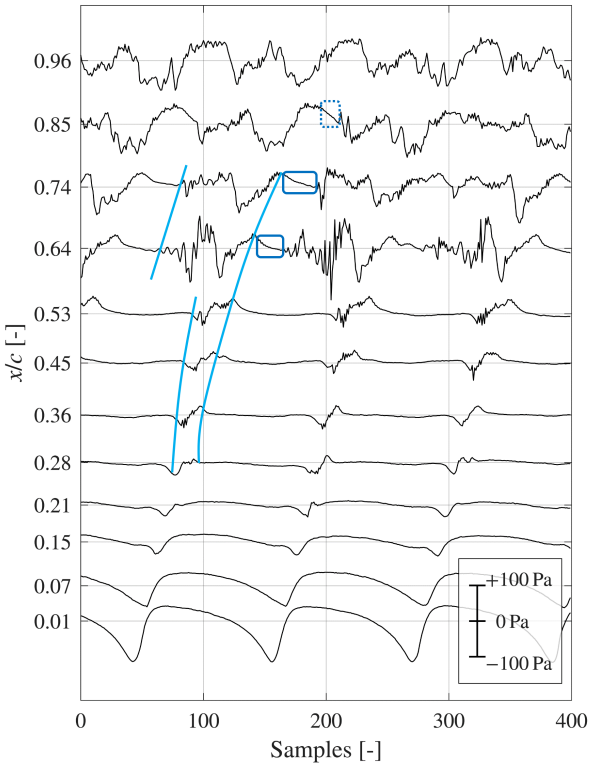


Fig. 8: Pressure signal of different sensors, Propeller 1, $y/R = 0.5$

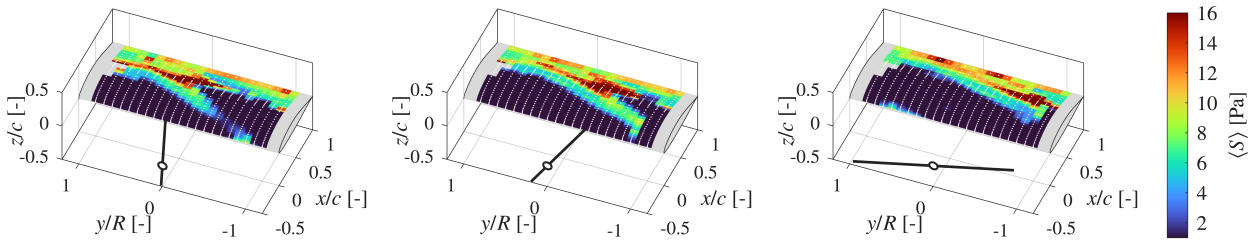
tire cycle, with no areas of lower fluctuations in between. The spreading of the high-fluctuation areas seems to be wedge-shaped up to the chordwise position where transition in the steady reference case normally occurs. Downstream of this critical position, areas of high fluctuation are already present before the arrival of the propeller blade wake. Nevertheless, regions with a seemingly laminar flow exist even in this aft chord region, highlighted by the blue boxes in Figure 8. A possible explanation is provided by the so-called "calmed regions" that occur directly after the passage of the blade wakes.

To quantify the proportions of the different boundary-layer states, the moving scatter value S is now calculated as described in subsection 2.1.

Figure 9 shows the phase-averaged moving scatter $\langle S \rangle$ across the 3D wing for three different phase-angle intervals. The blade wake passage is easily recognizable by the increased scatter values. The influence of the blade tip vortices around $y/R = -0.8$ is particularly evident in the long streak of high scatter values. Similarly extended turbulent regions occur behind the rising propeller blade at $y/R = 0.7$ and $y/R = 0.8$, although they are not clearly discernible in the phase intervals shown here. The effect of the blade tip vortex seems to be stronger behind the descending propeller blade than behind the rising blade. These scatter values provide a first visible indication of how the disturbances introduced by the propeller move across the wing.

To better understand the interactions at the wing surface, a different representation is used. It shows the same phase-averaged moving scatter $\langle S \rangle$ at a single spanwise position but across all phase bins of a complete propeller rotation. The representative position of $y/R = 0.5$ is chosen because the blade wakes are pronounced at this location, whereas the blade tip vortices do not have a visible influence. Thus, the effects of the blade wake alone can be investigated in isolation.

As shown in Figure 10, the calmed region, indicated by the low scatter values immediately after the passing of the blade wake, exists for a short period of time. Within this region, the turbulence seems to be suppressed, as substantially higher scatter values



(a) $\phi = 0°...6°$ **(b)** $\phi = 30°...36°$ **(c)** $\phi = 72°...78°$

Fig. 9: Phase-averaged scatter $\langle S \rangle$ of the residual pressure, Propeller 1

would be expected during transition and in a fully turbulent boundary layer.

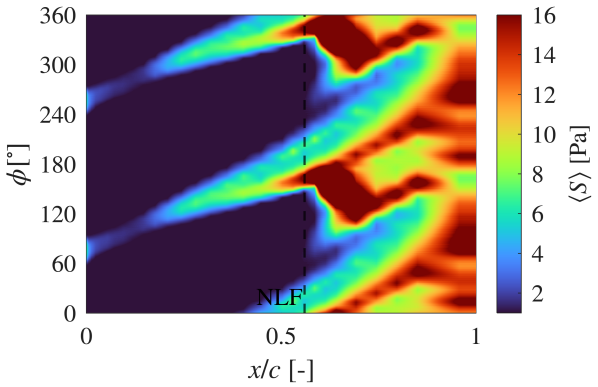


Fig. 10: Evolution of the phase-averaged scatter values, Propeller 1, $y/R = 0.5$

Another aspect not yet discussed is the role of the laminar separation bubble present in the steady reference configuration. The separation bubble extends approximately from $x/c \approx 56\,\%$ to $x/c \approx 63\,\%$ and ultimately leads to a turbulent boundary layer upon reattachment. In the reference configuration, the transition over the bubble appears as a region of very high scatter, exceeding values of $\langle S \rangle > 40\,Pa$. Downstream of the bubble, in the transitioned turbulent flow, the scatter values decrease markedly to $\langle S \rangle < 10\,Pa$ before gradually increasing again toward the trailing edge.

In the displayed propeller case, the region with scatter values of $\langle S \rangle > 16\,Pa$, marked in dark red, corresponds to transitioning or strongly turbulent boundary-layer portions. As the calmed region disappears, *Gostelow and Thomas* [6] demonstrated that the flow eventually returns toward its undisturbed natural state if sufficient time elapses before the next blade wake arrives. The laminar separation bubble of the reference configuration would then likely reappear. Whether sufficient time elapses in this case for the high scatter values to indicate a reappearing separation bubble, or whether other mechanisms trigger transition after the passage of the calmed region, remains unclear given the measurement technique employed. What can be said is that in the regions of very low scatter indicating the calmed region, transition does not occur, either over a laminar separation bubble or through any other mechanism. The very high scatter values directly in the wake of the propeller blades at $x/c > 56\,\%$ could be caused by bypass transition that is already happening before. Here, too, however, the exact transition mechanisms cannot be determined for sure from the pressure measurements alone. Therefore, further boundary-layer measurements, using hot-wire probes, are necessary and planned for a future wind tunnel campaign.

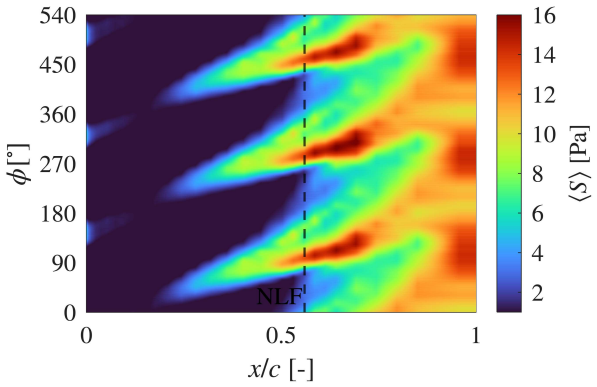


Fig. 11: Evolution of the phase-averaged scatter values, Propeller 2, $y/R = 0.5$

At higher blade-passing frequencies, as in the case of Propeller 2, the regions of very high scatter are smaller. Instead, in the downstream regions of the profile, broader areas exhibiting mid- to high-level scatter are present. This is visible in Figure 11. The calmed region in the downstream portion of the airfoil is significantly smaller than that in the wake of Propeller 1.

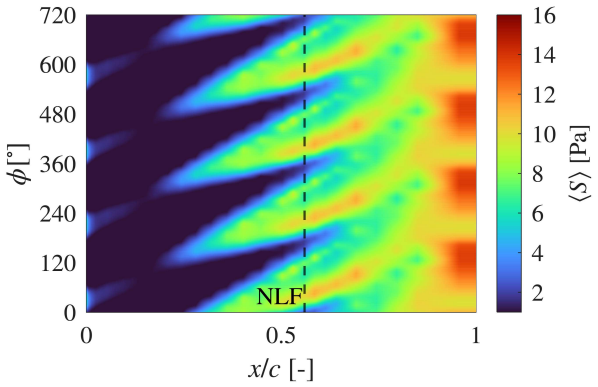


Fig. 12: Evolution of the phase-averaged scatter values, Propeller 3, $y/R = 0.5$

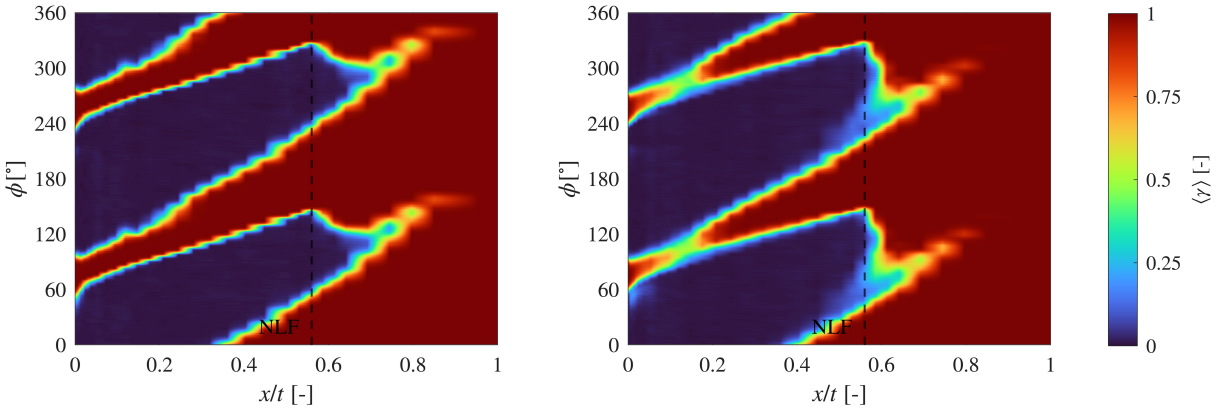
For Propeller 3, shown in Figure 12, regions of very high scatter are no longer observed. In this case, a possible transition in between the individual blade wakes seems to be suppressed. This would be consistent with the wakes of Propeller 3 merging into a single fully turbulent boundary-layer region caused by bypass transition before reaching the chordwise position of the laminar separation bubble where transition occurs in the steady reference case. This merging effect is shown and explained later in Figure 13. Nevertheless, it should be noted that at blade-passing frequencies as high as those of Propeller 3, the broader regions of lower scatter values could also be a side effect of how the moving scatter values are calculated. While the chosen window of 11 samples is sufficient to isolate regions of very high scatter if they persist for a sufficiently long time, short-lived regions could be smeared by the calculation, resulting in lower detected scatter values spread over broader phase intervals.

The boundary-layer states can be determined using the threshold of $S = 1.25\,Pa$ derived from the reference configurations. This operation is applied to each sample in each phase bin, yielding the phase averaged intermittency $\langle\gamma\rangle$ as the portion of samples within each phase bin with scatter values above the threshold. Of particular interest is the behaviour across all phase angles in the regions dominated by the blade tip vortex, compared to the inner radial regions, where the blade wake has the main impact on the boundary layer. Additionally, the effects of the three different propellers must be compared again to provide an overall picture.

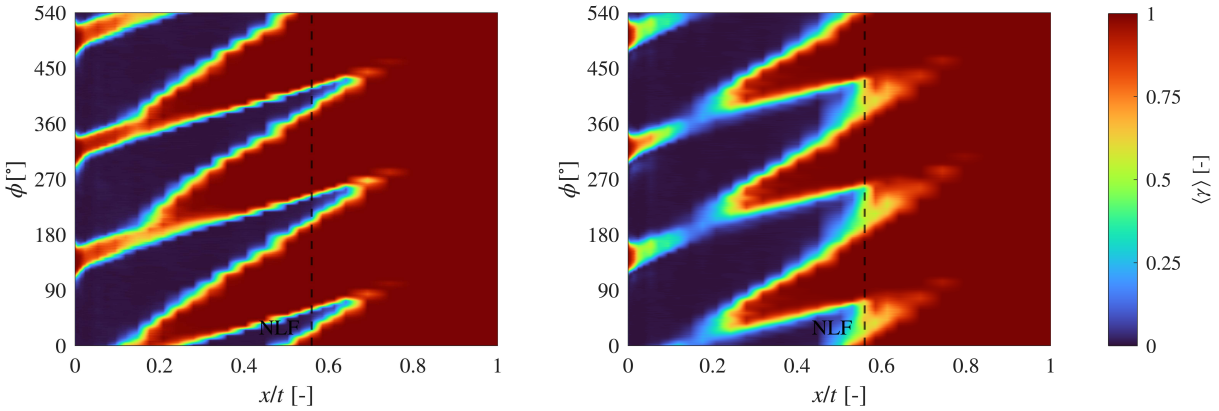
Looking at Figure 13, the calmed region is mainly visible at downstream chordwise positions for the first and second propeller. In the chordwise regions upstream of the natural transition point, the calmed region cannot be distinguished from the natural laminar flow, and its existence there is therefore not demonstrated in this study. Where present, in the blade-tip-vortex-dominated region at $y/R = 0.7$, the calmed region is much more pronounced than in the inner region of the wing at $y/R = 0.5$. This is seen in Figure 13 (a), (b), (c) and (d). The higher disturbance amplitude of the blade tip vortices leads to larger, meaning longer lasting turbulent areas upstream, whereas downstream, the calmed region after a passing large disturbance seems to be more stable, thus lasting longer before collapsing. Intermittently, laminar flow extends up to 80 % of the chord behind the first propeller in the tip-vortex area. By comparison, without a propeller, laminar flow extends to approximately 56 % of the chord. These extremely long laminar extents, associated with the calmed region, persist only briefly before the laminar extent retreats, seemingly towards its natural value. Before the natural or clean state is reached, the next wake approaches and induces turbulence once again. At higher rotational speeds or lower advance ratios, as with Propellers 2 and 3, the blade wakes and blade tip vortices pass at a higher frequency. Thus, their spatial distance or separation is also smaller. Because of their wedge shape, the edges of the turbulent regions move closer together as they advance over the airfoil, eventually merging into one turbulent area. In the cases investigated, the higher the blade pass frequency, the earlier the wake-induced turbulent wedges merge into one turbulent area. The wedges themselves are narrower at higher rotational speeds, leading to smaller turbulent areas at early chordwise positions on the wing.

This is consistent with the turbulence intensities in the propeller wakes reported by *Konrad et al.* [13]. They found that with higher rotational speeds, and thus lower advance ratios, the turbulent regions of the blade wakes exhibit lower turbulence intensities. Apparently, these low levels of freestream turbulence impinging on the airfoil are insufficient to induce early bypass transition in the highly stable upstream regions of the airfoil, where the pressure gradient is strongly favourable.

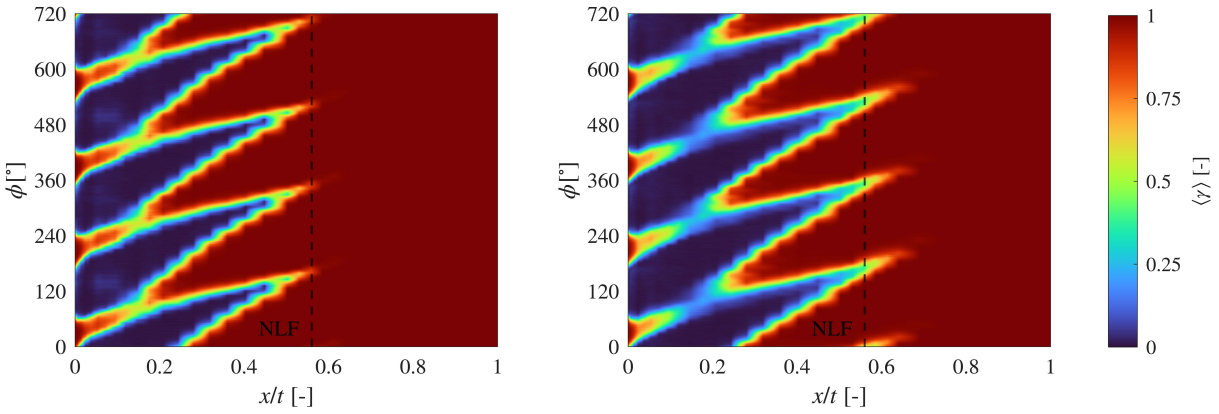
Time-averaging the intermittency values shown in Figure 13 for each grid point reveals different trends in the upstream and downstream regions of the airfoil. Upstream, Propeller 1 produces the highest intermittency, whereas Propeller 2 produces the lowest. Although the wakes of Propeller 3 are much weaker than those of Propeller 1 and slightly weaker than those of Propeller 2, their closer spacing appears to result in higher time-averaged intermittency than for Propeller 2. This suggests a trade-off be-



(a) Propeller 1, $y/R = 0.7$ **(b)** Propeller 1, $y/R = 0.5$



(c) Propeller 2, $y/R = 0.7$ **(d)** Propeller 2, $y/R = 0.5$



(e) Propeller 3, $y/R = 0.7$ **(f)** Propeller 3, $y/R = 0.5$

Fig. 13: Intermittency $\langle\gamma\rangle$ changing over the phase angle for different propellers at two spanwise positions

tween stronger, less frequent wakes at lower blade-passing frequencies and weaker, more frequent wakes at higher blade-passing frequencies.

The upstream trend does not, however, imply that Propeller 2 has the lowest intermittency across the entire airfoil. Downstream, Propeller 1 produces lower intermittency than the other two propellers: its wakes are more widely spaced, while their growth rate is similar to that of the other wakes. These results suggest that increasing rotational speed is beneficial to the portion of laminar flow upstream only up to a point, whereas lower rotational speeds appear most beneficial downstream.

For a global evaluation of the different effects, the intermittency is now averaged not only over time but also over the entire chord, from $x/c = [0, 1]$, and across the spanwise range, from $y/R = [-1, 1]$. This yields a global intermittency value for the boundary layer behind each propeller. Table 2 lists the total laminar portion and its value relative to the undisturbed reference measurement for each case.

case	lam. [%]	lam/lam$_{clean}$ [%]
clean	54.5	100
Propeller 1	44.1	80.9
Propeller 2	39.1	71.7
Propeller 3	34.5	63.3

Tab. 2: Total averaged laminar portion of the boundary layer

These values are significant. For the first propeller, the laminar portion exceeds 80 % of that in the undisturbed reference case. Such a high laminar portion suggests a substantial reduction in skin-friction drag compared with a fully turbulent or early-transitioning boundary layer. Thus still retaining much of the drag advantage of the NLF airfoil within the slipstream. Nevertheless, the boundary-layer velocity profiles in the regions identified here as laminar remain unknown because they cannot be determined from this type of measurements. A fuller, more stable velocity profile, as suspected in the calmed region, could result in greater wall shear stress and thus an increased friction drag compared to a natural laminar boundary layer. Therefore, this study alone does not permit a quantitative assessment of total drag or the associated drag advantage. It does, however, show that the configuration with the highest advance ratio and therefore the lowest blade-passing frequency has the greatest total laminar extent. In the cases investigated, increasing the blade-passing frequency increases the turbulent portion of the boundary layer.

4 Conclusion

This study confirms the existence of significant laminar boundary layer portions on an airfoil in the propeller slipstream under suitable conditions. The assumption of fully turbulent flow in the slipstream, which is frequently made during design, is therefore overly conservative. The occurrence of laminar and turbulent boundary layer portions is of a periodic or cyclic nature, matching the blade pass frequency, as already observed by *Miley et al.* [15].

In the configurations investigated in this study, the blade-passing frequency, and thus the frequency at which blade wakes encounter the airfoil, emerged as a key factor influencing the extent of laminar flow. Of the three configurations investigated, Propeller 1, with the lowest blade-passing frequency and the highest advance ratio, proved the most favorable. It exhibited both the longest transient laminar-flow extents and the greatest time-averaged laminar boundary-layer coverage. In this case, the average laminar-flow extent still reached approximately 80 % of that in the undisturbed reference configuration without a propeller. Calmed regions were most clearly identifiable and most pronounced downstream of Propeller 1.

The evaluated data strongly indicate that the laminar separation bubble, present in the steady reference case, is suppressed in the calmed region and possibly in the blade wake itself. At sufficiently low blade-passing frequencies, a laminar separation bubble may occur intermittently between the end of the calmed region and the arrival of the next blade wake, although it cannot be distinguished from other transition mechanisms using the present measurement setup. At higher blade-passing frequencies, as for Propeller 2, transition regions in between the calmed region and the following propeller blade appear to be smaller; for Propeller 3, transition mechanisms other than the wake-induced bypass transition seem to be suppressed throughout the propeller cycle.

The measurements conducted in this study alone did not permit a quantitative assessment of the drag reduction relative to a fully turbulent boundary layer. Further boundary-layer investigations using more precise measurement techniques, such as hot-wire anemometry, are required for this purpose and have already been planned. They will also enable a more precise characterization of the boundary-layer states and transition mechanisms than surface pressure measurements. Nevertheless, the measured results strongly suggest lower skin-friction drag than that of a fully turbulent boundary layer.

References

[1] Borer, N., Patterson, M., Viken, J., Moore, M., Bevirt, J., Stoll, A., and Gibson, A., Design and performance of the nasa sceptor distributed electric propulsion flight demonstrator, 06 2016, DOI: 10.2514/6.2016-3920.

[2] Catalano, F. M., On the effects of an installed propeller slipstream on wing aerodynamic characteristics, *Acta Polytechnica*, 44(3), Jan. 2004, ISSN: 1210-2709, DOI: 10.14311/562.

[3] Deere, K. A., Viken, S., Carter, M., Viken, J. K., Wiese, M., and Farr, N., *Computational Analysis of Powered Lift Augmentation for the LEAPTech Distributed Electric Propulsion Wing*, In *35th AIAA Applied Aerodynamics Conference*, 2017, DOI: 10.2514/6.2017-3921.

[4] Elsaadawy, E. and Britchert, C., The extent of a laminar boundary layer under the influence of a propeller slipstream, *20th AIAA Applied Aerodynamics Conference*, 01 2002.

[5] Englund, D. R. and Richards, B. W., The infinite line pressure probe, Technical Memorandum 83582, NASA, 1984.

[6] Gostelow, J. P. and Thomas, R. L., Response of a laminar separation bubble to an impinging wake, *Journal of Turbomachinery*, (127):35–42, 2005, DOI: 10.1115/1.1829729.

[7] Gostelow, J. P., Walker, G. J., Solomon, W. J., Hong, G., and Melwani, N., Investigation of the calmed region behind a turbulent spot, *Journal of Turbomachinery*, (119):802–809, 1997, DOI: 10.1115/1.2841191.

[8] Halstead, D. E., Wisler, D. C., Okiishi, T. H., Walker, G. J., Hodson, H. P., and Shin, H.-W., Boundary layer developement in axial compressors and turbines: Part 1 of 4 - composite picture, *Journal of Turbomachinery*, (119):114–127, 1997.

[9] Hood, M. J. and Gaydos, E. M., Effects of propellers and of vibration on the extent of laminar flow on the naca 27-212 airfoil, Wartime Report, 1939.

[10] Horstmann, K.-H., Müller, R., Rohardt, C.-H., Quast, A., Wolrath, W., Echtle, H., Dick, P., Welte, D., Stock, H. W., and Moeken, B., Design and flight test evaluation of a laminar wing glove on a commuter aircraft, *ICAS*, 1994.

[11] Hussain, F. and Reynolds, W., The mechanics of an organized wave in turbulent shear flow, *Journal of Fluid Mechanics*, 41:241–258, 1970, DOI: 10.1017/S0022112070000605.

[12] Kim, H. D., Perry, A. T., and Ansell, P. J., *A Review of Distributed Electric Propulsion Concepts for Air Vehicle Technology*, In *2018 AIAA/IEEE Electric Aircraft Technologies Symposium*, 2018, DOI: 10.2514/6.2018-4998.

[13] Konrad, N., Schollenberger, M., Deck, U., and Lutz, T., Measurements of the development of the velocity fields in a propeller wake, Oct. 2026, DOI: 10.21203/rs.3.rs-10918041/v1.

[14] Kuhn, A., Nussbaumer, E., Denzel, J., Bergmann, D., and Strohmayer, A., Modification of a scaled flight demonstrator for the implementation and experimental investigation of an energy harvesting powertrain in distributed electric propulsion systems, *Aerospace*, 13:435, 05 2026, DOI: 10.3390/aerospace13050435.

[15] Miley, S. J., Howard, R. M., and Holmes, B. J., Wing laminar boundary layer in the presence of a propeller slipstream, *Journal of Aircraft*, 25(7):606–611, 1988, ISSN: 0021-8669, DOI: 10.2514/3.45630.

[16] Prandtl, L., Mutual influence of wings and propeller, *Technical Report*, 1921.

[17] Schubauer, G. B. and Klebanoff, P. S., Contributions on the mechanics of boundary-layer transition, Report 1289, 1955.

[18] Seyfert, D. P., Deck, U., and Geiger, J., Unsteady effects of a tractor propeller on a laminar wing: an experimental setup, DOI: 10.25967/630099.

[19] Wenzinger, C. J., Wind tunnel investigations of several factors affecting the performance of a high speed pursuit airplane with air-cooled engine, *NACA Advance Confidential Report*, November 1941.

[20] Zalovcik, J. A. and Skoog, R. B., Flight investigation of boundary-layer transition and profile drag of an experimental low-drag wing installed on a fighter-type airplane, Wartime Report, 1945.